JHEP

Published for SISSA by Springer

Received: August 9, 2012
Revised: December 9, 2012
Accepted: December 13, 2012
Published: January 22, 2013

NLO QCD matrix elements + parton showers in $e^+e^- \to$ hadrons

Thomas Gehrmann,[a] **Stefan Höche,**[b] **Frank Krauss,**[c] **Marek Schönherr**[c] **and Frank Siegert**[d]

[a] *Institut für Theoretische Physik, Universität Zürich, Winterthurerstrasse 190, CH-8057 Zürich, Switzerland*

[b] *SLAC National Accelerator Laboratory, 2575 Sand Hill Rd, Menlo Park, CA 94025, U.S.A.*

[c] *Institute for Particle Physics Phenomenology, Durham University, South Rd, Durham DH1 3LE, U.K.*

[d] *Physikalisches Institut, Albert-Ludwigs-Universität Freiburg, Hermann-Herder-Str. 3, D-79104 Freiburg, Germany*

E-mail: thomas.gehrmann@uzh.ch, shoeche@slac.stanford.edu, frank.krauss@durham.ac.uk, marek.schoenherr@durham.ac.uk, frank.siegert@cern.ch

Abstract: We present a new approach to combine multiple NLO parton-level calculations matched to parton showers into a single inclusive event sample. The method provides a description of hard multi-jet configurations at next-to leading order in the perturbative expansion of QCD, and it is supplemented with the all-orders resummed modelling of jet fragmentation provided by the parton shower. The formal accuracy of this technique is discussed in detail, invoking the example of electron-positron annihilation into hadrons. We focus on the effect of renormalisation scale variations in particular. Comparison with experimental data from LEP underlines that this novel formalism describes data with a theoretical accuracy that has hitherto not been achieved in standard Monte Carlo event generators.

Keywords: Monte Carlo Simulations, NLO Computations

ArXiv ePrint: 1207.5031

doi:10.1007/JHEP01(2013)144

JHEP01(2013)144

Contents

JHEP01(2013)144

1 Introduction

During the past decade, Monte-Carlo methods for simulating hadronic final states in collider experiments have improved continuously. Multi-purpose event generators incorporating the most recent higher-order perturbative QCD calculations have thus emerged, making them available to phenomenology and experiment alike. This has far-reaching consequences for both precision physics and searches for new phenomena. Key to the developments has been the steady progress in understanding the interplay of real and virtual higher-order QCD corrections on one hand and of resummation techniques like parton-shower algorithms on the other hand. The construction and development of simulation tools for QCD processes has become one of the central activities of research in collider phenomenology.

This publication discusses an extension to the established techniques of multi-jet merging and next-to-leading order matrix-element matching. Existing multi-jet merging methods (MEPS) combine leading-order matrix elements of varying final-state multiplicity with parton showers. They were pioneered in [1–4] and further matured in [5–8]. The key advantage of these methods is the possibility to describe arbitrarily complex final states at

leading order in the strong coupling, while providing fully inclusive event samples with resummation effects taken into account. They have therefore become standard analysis tools for collider experiments. However, they lack the precision of a full next-to-leading order perturbative calculation. This is remedied by next-to-leading order matrix-element matching methods (MC@NLO), which combine NLO QCD calculations of fixed jet multiplicity with parton showers. They were introduced in [9, 10] and have recently been automated in various programs [11, 12]. Their main advantage lies in the excellent description of well-defined, inclusive final states. Using the MENLOPS technique [13, 14], it is possible to make these results exclusive and combine them with higher-multiplicity leading-order predictions in order to recover the virtues of MEPS methods.

The aim of this paper is to further improve upon the existing algorithms and construct a consistent, process-independent merging method for matched NLO predictions with varying jet multiplicity. Pictorially speaking, we intend to replace the leading-order matrix elements of the original MEPS approach with corresponding ones at next-to-leading order. This is achieved by combining various MC@NLO event samples and accounting for potential double counting by means of a modified truncated parton shower [5, 10]. Ultimately, we intend to maintain the fixed-order accuracy of the matrix elements, but also to preserve the logarithmic accuracy of the parton shower. The new method discussed here goes well beyond the scope of the MENLOPS technique.

In the framework of this paper the formalism is specified for a multi-jet merging at NLO accuracy for e^+e^--annihilations into hadrons, building on the existing implementations of MEPS [5] and MC@NLO [12] techniques in the SHERPA event generator [15, 16]. In the present paper, however, we will assume that the evolution parameter of the parton shower is defined in such a way, equivalent to the measure of hardness of a parton splitting, that effects due to a mismatch of these two quantities can be neglected. In other words we will neglect effects that arise from allowed emissions generated by truncated parton showers. An algorithm with the same goals and a similar setup for the parton shower has been detailed, also for e^+e^--annihilations into hadrons, in [17]. A method for merging NLO vector boson plus 0 and 1-jet samples was introduced in [18], while [19] proposed a general method for NLO vector boson production plus n jets and implemented it for n=0,1,2. Here we apply the method of [19] to hadronic final states in e^+e^--annihilation.

The outline of the present paper is as follows: section 2 discusses the MEPS algorithm for matrix-element merging at leading order, and the MC@NLO method for NLO matching as implemented in SHERPA. As an intermediate step, the implementation of the MENLOPS idea for MC@NLO core processes is presented. With the notation thus established, the new merging method at next-to leading order, MEPS@NLO, is introduced in section 3. The renormalisation scale dependence of the result is discussed in some detail. Section 4 is devoted to details of the Monte-Carlo implementation. Example results for the case of electron-positron annihilation into hadrons are shown in section 5, including the impact of scale variations and of varying the number of jets described by NLO matrix element calculations. Section 6 presents our conclusions.

JHEP01(2013)144

2 Brief review of merging and matching techniques

In this section, existing matrix-element parton-shower merging and matching methods are briefly reviewed, using the notation of [12]. As already stated in the introduction, the effects of allowed emissions generated by truncated showers [5, 10] are ignored, which improves the readability of this publication, allowing to focus on the structure of the result. For a full algorithmic solution, we refer to the parallel publication, in [19]. Our approach is justified by the choice of transverse momentum as evolution variable in the parton shower used for this publication.

In the context of merging, we define a jet criterion Q_n, which typically denotes the minimal value of some relative transverse momentum present in the n-parton phase-space configuration Φ_n. Correspondingly, Q_{cut} denotes a jet-defining cut value, called the merging scale, such that for n-jet events the condition $Q_n > Q_{\text{cut}}$ is fulfilled.[1]

Formally, the quantity of interest is the expectation value $\langle O \rangle$ of an arbitrary, infrared-safe observable O, evaluated by taking the average over sufficiently many points in an n-particle phase-space, Φ_n.

The methods reviewed here, as well as our newly proposed technique, have the following aims

- multi-jet merging techniques.
  For configurations with n jets, the respective fixed-order accuracy of $\langle O \rangle$ inherent to the parton-level result should be maintained. More precisely, for leading-order merging (MEPS), jet observables for n jets above the merging scale Q_{cut} should be determined at leading-order accuracy. For next-to-leading order merging (MEPS@NLO) they should be given at NLO accuracy. For configurations below Q_{cut}, the MEPS accuracy will be that of the parton shower, while for MEPS@NLO leading-order accuracy is envisaged. At the same time we require that the logarithmic accuracy of the shower be either maintained or improved in the region above Q_{cut}.

- NLO matching methods.
  For processes leading to n-parton final states at leading order all n-particle inclusive observables, and in particular the total cross section, are expected to reproduce the fixed order NLO results. At the same time, all $n+1$-particle observables are expected to be given at leading order accuracy, while higher-order emissions should still be described by the leading logarithmic approximation of the parton shower.

[1] The jet criterion Q applied here has been slightly modified compared to [5], in order to reflect the fact that no unique parton flavour can be assigned at the next-to-leading order. For any pair of final-state partons i and j we define

$$Q_{ij}^2 \;=\; 2\,p_i p_j \,\min_{k\neq i,j}\,\frac{2}{C_{i,j}^k + C_{j,i}^k} \qquad \text{where} \qquad C_{i,j}^k \;=\; \frac{p_i p_k}{(p_i + p_k) p_j}\,. \tag{2.1}$$

The spectator index k runs over all possible coloured particles.

JHEP01(2013)144

2.1 Leading-order merging — MEPS

In the context of the leading-order merging method proposed in [5], the following quantities are introduced:

- squared leading-order (Born) matrix elements, $\mathrm{B}_n(\Phi_n)$, for n outgoing particles, summed (averaged) over final state (initial state) spins and colours and including symmetry and flux factors.

- Sudakov form factors of the parton shower, given by

$$\Delta_n^{(\mathrm{PS})}(t,t') = \exp\left\{ -\int_t^{t'} \mathrm{d}\Phi_1 \; \mathrm{K}_n(\Phi_1) \right\}, \tag{2.2}$$

  K_n denotes the sum of all splitting kernels for the n-body final state. The one-particle phase-space element for a splitting, $\mathrm{d}\Phi_1$, is parametrised as

$$\mathrm{d}\Phi_1 \;=\; \mathrm{d}t\,\mathrm{d}z\,\mathrm{d}\phi \;\; J(t,z,\phi)\;, \tag{2.3}$$

  where t is the ordering variable, z is the splitting variable and ϕ is the azimuthal angle. $J(t,z,\phi)$ is the appropriate Jacobian factor. The ordering variable is usually taken to fulfil $t \propto k_\perp^2$ as $t \to 0$.

- The resummation scale μ_Q, which defines an upper limit of parton evolution in terms of the shower evolution variable. t_c is an infrared regulator of the order of Λ_{QCD} marking the transition into the non-perturbative region.

The expectation value of an arbitrary, infrared-finite observable O, leading order for n partons, to $\mathcal{O}(\alpha_s)$ has been computed in [14]. It is derived from the following expression:

$$\begin{aligned}\langle O\rangle = &\int \mathrm{d}\Phi_n \mathrm{B}_n(\Phi_n) \left[\Delta_n^{(\mathrm{PS})}(t_c,\mu_Q^2)\, O(\Phi_n) + \int_{t_c}^{\mu_Q^2} \mathrm{d}\Phi_1 \; \mathrm{K}_n(\Phi_1)\, \Delta_n^{(\mathrm{PS})}(t_{n+1},\mu_Q^2)\, \Theta(Q_{\mathrm{cut}} - Q_{n+1})\; O(\Phi_{n+1}) \right] \\ &+ \int \mathrm{d}\Phi_{n+1}\; \mathrm{B}_{n+1}(\Phi_{n+1})\, \Delta_n^{(\mathrm{PS})}(t_{n+1},\mu_Q^2)\, \Theta(Q_{n+1} - Q_{\mathrm{cut}})\; O(\Phi_{n+1})\;, \end{aligned} \tag{2.4}$$

where $O(\Phi_m)$ is the observable evaluated for an m-parton final state. The square bracket on the first line and the Sudakov factor on the second line are both generated by the parton shower, while the terms $\mathrm{d}\Phi_n \mathrm{B}_n$ and $\mathrm{d}\Phi_{n+1}\mathrm{B}_{n+1}$ correspond to the fixed-order event generation. The term on the second line yields leading-order accuracy for any $n+1$-particle observable in the region $Q_{n+1} > Q_{\mathrm{cut}}$. Leading-order accuracy for observables sensitive to Φ_n is guaranteed by the fact that eq. (2.4) can be rewritten as

$$\begin{aligned}\langle O\rangle = &\int \mathrm{d}\Phi_n\; \mathrm{B}_n(\Phi_n) \left[\Delta_n^{(\mathrm{PS})}(t_c,\mu_Q^2)\, O(\Phi_n) + \int_{t_c}^{\mu_Q^2} \mathrm{d}\Phi_1 \; \mathrm{K}_n(\Phi_1)\, \Delta_n^{(\mathrm{PS})}(t_{n+1},\mu_Q^2)\; O(\Phi_{n+1}) \right] \\ &+ \int \mathrm{d}\Phi_{n+1} \Big[\mathrm{B}_{n+1}(\Phi_{n+1}) - \mathrm{B}_n(\Phi_n)\, \mathrm{K}_n(\Phi_{n+1}) \Big] \Delta_n^{(\mathrm{PS})}(t_{n+1},\mu_Q^2)\, \Theta(Q_{n+1} - Q_{\mathrm{cut}}) O(\Phi_{n+1})\;, \end{aligned} \tag{2.5}$$

JHEP01(2013)144

where the first line is the $\mathcal{O}(\alpha_s)$ parton-shower result [20] and independent of Q_{cut}. The additional terms on the second line incorporate possible sub-leading colour single logarithms as well as power corrections. The size of these corrections determines the potential discontinuity in $\langle O \rangle$ at Q_{cut}. It can be large if Q_{cut} is either far from the collinear limit or sub-leading colour single logarithms are important. Sub-leading colour configurations, however, can be included in a systematic manner, as was detailed in [12].

An important feature of eq. (2.4) is that it can be iterated to incorporate higher-multiplicity leading-order matrix elements into the prediction. By replacing $n \to n+1$, all properties of the algorithm remain the same. In order to obtain this property when dealing with next-to-leading order matrix elements, a slight modification is necessary, which will be described in section 3.

2.2 Next-to-leading order matching — MC@NLO

In the MC@NLO matching method the following additional quantities are needed:

- squared real-emission matrix elements, $\mathrm{R}_n(\Phi_{n+1})$, for n-particle processes, summed (averaged) over final state (initial state) spins and colours and including symmetry and flux factors. Note that $\mathrm{R}_n(\Phi_{n+1}) = \mathrm{B}_{n+1}(\Phi_{n+1})$.

- The NLO-weighted Born differential cross section $\bar{\mathrm{B}}_n^{(\mathrm{A})}$, defined as

$$\begin{aligned} \bar{\mathrm{B}}_n^{(\mathrm{A})}(\Phi_n) &= \mathrm{B}_n(\Phi_n) + \mathrm{V}_n(\Phi_n) + \mathrm{I}_n^{(\mathrm{S})}(\Phi_n) \\ &\quad + \int \mathrm{d}\Phi_1 \left[\mathrm{D}_n^{(\mathrm{A})}(\Phi_{n+1})\, \Theta(\mu_Q^2 - t_{n+1}) - \mathrm{D}_n^{(\mathrm{S})}(\Phi_{n+1}) \right] . \end{aligned} \tag{2.6}$$

  Here, V_n is the Born-contracted one-loop amplitude, and $\mathrm{I}_n^{(\mathrm{S})}$ is the sum of integrated subtraction terms, cf. [12], while $\mathrm{D}_n^{(\mathrm{S})}$ are the corresponding real subtraction terms. In contrast, $\mathrm{D}_n^{(\mathrm{A})}$ are the MC@NLO evolution kernels multiplied by Born matrix elements. Both functions can be decomposed in terms of dipole contributions, $\mathrm{D} = \sum_{ij,k} \mathrm{D}_{ij,k}$, where each dipole encodes exactly one singular region [12]. Further, each dipole has a corresponding phase space factorisation $\mathrm{d}\Phi_{n+1} = \mathrm{d}\Phi_n\, \mathrm{d}\Phi_1^{ij,k}$ and $t_{n+1} = t(\Phi_{n+1})$ is defined in terms of eq. (2.3) in each of these dipole phase spaces.

- The hard remainder function

$$\mathrm{H}_n^{(\mathrm{A})}(\Phi_{n+1}) \;=\; \mathrm{R}_n(\Phi_{n+1}) - \mathrm{D}_n^{(\mathrm{A})}(\Phi_{n+1})\, \Theta(\mu_Q^2 - t_{n+1}) \,, \tag{2.7}$$

  with $t_{N+1} = t(\Phi_{n+1})$ defined as above.

- The MC@NLO Sudakov form factor

$$\Delta_n^{(\mathrm{A})}(t, t') \;=\; \exp\left\{ -\int_t^{t'} \mathrm{d}\Phi_1\, \frac{\mathrm{D}_n^{(\mathrm{A})}(\Phi_n, \Phi_1)}{\mathrm{B}(\Phi_n)} \right\} , \tag{2.8}$$

  Note that $\Delta_n^{(\mathrm{A})}$ implicitly depends on Φ_n, while the original Sudakov form factor $\Delta_n^{(\mathrm{PS})}$ does not. This is a consequence of the fact that the two Sudakov form factors

JHEP01(2013)144

differ by their treatment of colour and spin correlations and it was discussed in detail in [12]. By incorporating full colour information in $\mathrm{D}^{(\mathrm{A})}$, it is easily possible to obtain the exact same singularity structure as in the real-emission matrix element [21, 22].

The expectation value of an arbitrary infrared safe observable O to $\mathcal{O}(\alpha_s)$ is then given by [9]

$$\begin{aligned}\langle O\rangle = &\int \mathrm{d}\Phi_n\, \bar{\mathrm{B}}_n^{(\mathrm{A})}(\Phi_n)\left[\Delta_n^{(\mathrm{A})}(t_c,\mu_Q^2)\, O(\Phi_n) + \int_{t_c}^{\mu_Q^2}\mathrm{d}\Phi_1\, \frac{\mathrm{D}_n^{(\mathrm{A})}(\Phi_n,\Phi_1)}{\mathrm{B}_n(\Phi_n)}\, \Delta_n^{(\mathrm{A})}(t_{n+1},\mu_Q^2)\, O(\Phi_{n+1})\right] \\ &+ \int \mathrm{d}\Phi_{n+1}\, \mathrm{H}_n^{(\mathrm{A})}(\Phi_{n+1})\; O(\Phi_{n+1})\,.\end{aligned} \tag{2.9}$$

The square bracket on the first line is generated by a weighted parton shower, which will be discussed in section 4.2, while the terms $\mathrm{d}\Phi_n \bar{\mathrm{B}}_n^{(\mathrm{A})}$ and $\mathrm{d}\Phi_{n+1}\mathrm{H}_n^{(\mathrm{A})}$ correspond to fixed-order events. Events generated according to the first line are referred to as standard, or $\mathbb{S}$-events, while events generated according to the second line, the hard remainder, correspondingly are dubbed $\mathbb{H}$-events [9, 12]. Note that the square bracket in the first line integrates to one, reflecting the probabilistic nature of the Sudakov form factor. This, together with equations (2.6) and (2.7), implies that the total cross section reproduces the exact NLO result. Correspondingly, an MC@NLO prediction is next-to-leading order accurate for observables sensitive to the Born phase-space variables Φ_n, and leading-order accurate for observables sensitive to Φ_{n+1}. In contrast to the MEPS method, leading-order accuracy is maintained throughout the $n+1$-particle phase space, but it cannot be extended to higher parton or jet multiplicity. This extension will be the topic of section 2.3.

2.3 Combining NLO matching and LO merging — MENLOPS

NLO-matched predictions as described in section 2.2 can easily be merged with higher-multiplicity event samples at leading order accuracy using the techniques described in section 2.1. The original algorithm, based on the POWHEG method [10, 23], was independently proposed in [13] and [14]. In this publication we extend the method to MC@NLO, which requires the introduction of the local K-factor

$$k_n^{(\mathrm{A})}(\Phi_{n+1}) \;=\; \frac{\bar{\mathrm{B}}_n^{(\mathrm{A})}(\Phi_n)}{\mathrm{B}_n(\Phi_n)}\left(1-\frac{\mathrm{H}_n(\Phi_{n+1})}{\mathrm{R}_n(\Phi_{n+1})}\right)+\frac{\mathrm{H}_n(\Phi_{n+1})}{\mathrm{R}_n(\Phi_{n+1})}\,. \tag{2.10}$$

It is motivated by the behaviour of the underlying MC@NLO event sample in terms of $\mathbb{S}$- and $\mathbb{H}$-events [9, 12]. In the limit $\mathrm{H}_n^{(\mathrm{A})} \to 0$, i.e. for configurations with a soft additional parton, we obtain $k_n^{(\mathrm{A})}(\Phi_{n+1}) \to \bar{\mathrm{B}}_n^{(\mathrm{A})}(\Phi_n)/\mathrm{B}_n(\Phi_n)$. In the limit $\mathrm{H}_n^{(\mathrm{A})} \to \mathrm{R}_n^{(\mathrm{A})}$, i.e. for configurations with a hard additional parton, we have instead $k_n^{(\mathrm{A})}(\Phi_{n+1}) \to 1$. Hence, the higher-multiplicity tree-level result is "scaled up" by the local K-factor from MC@NLO in the soft region, and it is left untouched in the hard region. In both cases, however, the n-parton phase-space configuration in eq. (2.10) is determined by backward clustering, as described in [5].

JHEP01(2013)144

The expectation value of an arbitrary, infrared-finite observable to $\mathcal{O}(\alpha_s)$ in the MENLOPS method for MC@NLO is given by

$$\begin{aligned}\langle O\rangle = &\int \mathrm{d}\Phi_n\, \bar{\mathrm{B}}_n^{(\mathrm{A})}(\Phi_n) \\ &\times \left[\Delta_n^{(\mathrm{A})}(t_c,\mu_Q^2)\, O(\Phi_n) + \int_{t_c}^{\mu_Q^2} \mathrm{d}\Phi_1 \frac{\mathrm{D}_n^{(\mathrm{A})}(\Phi_n,\Phi_1)}{\mathrm{B}_n(\Phi_n)} \Delta_n^{(\mathrm{A})}(t_{n+1},\mu_Q^2)\,\Theta(Q_{\mathrm{cut}}-Q_{n+1}) O(\Phi_{n+1})\right] \\ &+ \int \mathrm{d}\Phi_{n+1}\, \mathrm{H}_n^{(\mathrm{A})}(\Phi_{n+1})\, \Delta_n^{(\mathrm{PS})}(t_{n+1},\mu_Q^2)\,\Theta(Q_{\mathrm{cut}}-Q_{n+1})\; O(\Phi_{n+1}) \\ &+ \int \mathrm{d}\Phi_{n+1}\, k_n^{(\mathrm{A})}(\Phi_{n+1})\, \mathrm{B}_{n+1}(\Phi_{n+1})\, \Delta_n^{(\mathrm{PS})}(t_{n+1},\mu_Q^2)\,\Theta(Q_{n+1}-Q_{\mathrm{cut}})\; O(\Phi_{n+1})\,.\end{aligned} \tag{2.11}$$

This prediction is next-to-leading order accurate for observables sensitive to Φ_n and leading-order accurate for observables sensitive to Φ_{n+1}. The key advantage compared to a pure NLO-matched prediction is that final states of higher jet multiplicity are treated as in the MEPS approach. The improvement over results obtained by MEPS methods is the next-to leading order accuracy of the inclusive cross section and of observables sensitive to Φ_n.

The method aims to maintain the full NLO-accuracy in the n-jet phase space and the LO-accuracy in the $(n+1)$-jet phase space, without upsetting the logarithmic accuracy of the parton shower. In order to see that this indeed is the case, equation (2.11) can be rephrased as follows:

$$\langle O\rangle \;=\; \langle O\rangle^{\mathrm{MC@NLO}} \;+\; \langle O\rangle^{\mathrm{corr}}\,, \tag{2.12}$$

with $\langle O\rangle^{\mathrm{MC@NLO}}$ given by (2.9), and thus showing the desired property. It thus remains to show that the correction term does not introduce unwanted terms of higher logarithmic order. Omitting the obvious phase space arguments of the different matrix element contributions, it is given by

$$\begin{aligned}\langle O\rangle^{\mathrm{corr}} = &\int \mathrm{d}\Phi_{n+1}\,\Theta(Q_{n+1}-Q_{\mathrm{cut}})\, O(\Phi_{n+1})\, \Delta_n^{(\mathrm{PS})}(t_{n+1},\mu_Q^2) \\ &\quad\times\left\{\left[\frac{\bar{\mathrm{B}}_n^{(\mathrm{A})}}{\mathrm{B}_n}\left(1-\frac{\mathrm{H}_n^{(\mathrm{A})}}{\mathrm{B}_{n+1}}\right)+\frac{\mathrm{H}_n^{(\mathrm{A})}}{\mathrm{B}_{n+1}}\right]\mathrm{B}_{n+1}-\mathrm{H}_n^{(\mathrm{A})}-\frac{\bar{\mathrm{B}}_n^{(\mathrm{A})}}{\mathrm{B}_n}\mathrm{D}_n^{(\mathrm{A})}\frac{\Delta_n^{(\mathrm{A})}(t_{n+1},\mu_Q^2)}{\Delta_n^{(\mathrm{PS})}(t_{n+1},\mu_Q^2)}\right\} \\ = &\int \mathrm{d}\Phi_{n+1}\,\Theta(Q_{n+1}-Q_{\mathrm{cut}})\, O(\Phi_{n+1})\, \Delta_n^{(\mathrm{PS})}(t_{n+1},\mu_Q^2) \\ &\quad\times\left\{\frac{\bar{\mathrm{B}}_n^{(\mathrm{A})}}{\mathrm{B}_n}\mathrm{D}_n^{(\mathrm{A})}\left(1-\frac{\Delta_n^{(\mathrm{A})}(t_{n+1},\mu_Q^2)}{\Delta_n^{(\mathrm{PS})}(t_{n+1},\mu_Q^2)}\right)\right\}\end{aligned} \tag{2.13}$$

Since $\mathrm{D}_n^{(\mathrm{A})}$ is of $\mathcal{O}(\alpha_s L^2)$ and because the ratio of Sudakov form factor is at most of non-leading logarithmic order, $\mathcal{O}(\alpha_s L)$, and non-leading in $1/N_c$, the overall contribution of this term is at most of $\mathcal{O}(\alpha_s^2 L^3)$.[2] The logarithmic accuracy of the MENLOPS method therefore depends entirely on the logarithmic accuracy of the parton shower. If the parton shower is correct to NLL, the MENLOPS result will be as well. Hence, the MENLOPS technique will not impair the accuracy of the parton shower itself. Higher jet multiplicities exhibit the same accuracy as in the MEPS approach.

[2] This statement is based on the logarithmic accuracy of currently available parton showers. Parton showers which are extended to full NLL accuracy may become available in the future, in which case the mismatch of $\mathcal{O}(\alpha_s^2 L^3)$ would be absent.

JHEP01(2013)144

3 Merging at next-to leading order

The previous section sets the scene to introduce a new prescription, which consistently merges multiple MC@NLO-matched event samples of increasing jet multiplicity. The method is constructed such that it is next-to-leading order accurate for observables that are sensitive to both Φ_n and $\Phi_{n+1}\,\Theta(Q-Q_{\rm cut})$, while maintaining the logarithmic accuracy of MC@NLO for observables sensitive to Φ_{n+1}. In other words, the goal is to describe every jet observable at next-to leading order in the strong coupling constant, including Sudakov suppression factors.

3.1 Definition of the MEPS@NLO technique

We propose a method based on the following expression for the expectation value of an arbitrary infrared-finite observable O

$$
\begin{aligned}
\langle O\rangle = &\int \mathrm{d}\Phi_n\, \bar{\mathrm{B}}_n^{(\mathrm{A})} \left[\Delta_n^{(\mathrm{A})}(t_c,\mu_Q^2)\, O_n + \int_{t_c}^{\mu_Q^2} \mathrm{d}\Phi_1\, \frac{\mathrm{D}_n^{(\mathrm{A})}}{\mathrm{B}_n}\, \Delta_n^{(\mathrm{A})}(t_{n+1},\mu_Q^2)\Theta(Q_{\rm cut}-Q_{n+1})O_{n+1} \right] \\
&+ \int \mathrm{d}\Phi_{n+1}\, \mathrm{H}_n^{(\mathrm{A})}\, \Delta_n^{(\mathrm{PS})}(t_{n+1},\mu_Q^2)\, \Theta(Q_{\rm cut}-Q_{n+1})\, O_{n+1} \\
&+ \int \mathrm{d}\Phi_{n+1}\, \bar{\mathrm{B}}_{n+1}^{(\mathrm{A})} \left(1 + \frac{\mathrm{B}_{n+1}}{\bar{\mathrm{B}}_{n+1}^{(\mathrm{A})}} \int_{t_{n+1}}^{\mu_Q^2} \mathrm{d}\Phi_1\, \mathrm{K}_n \right) \Delta_n^{(\mathrm{PS})}(t_{n+1},\mu_Q^2)\, \Theta(Q_{n+1}-Q_{\rm cut}) \\
&\qquad \times \left[\Delta_{n+1}^{(\mathrm{A})}(t_c,t_{n+1})\, O_{n+1} + \int_{t_c}^{t_{n+1}} \mathrm{d}\Phi_1\, \frac{\mathrm{D}_{n+1}^{(\mathrm{A})}}{\mathrm{B}_{n+1}}\, \Delta_{n+1}^{(\mathrm{A})}(t_{n+2},t_{n+1})\, O_{n+2} \right] \\
&+ \int \mathrm{d}\Phi_{n+2}\, \mathrm{H}_{n+1}^{(\mathrm{A})}\, \Delta_{n+1}^{(\mathrm{PS})}(t_{n+2},t_{n+1})\, \Delta_n^{(\mathrm{PS})}(t_{n+1},\mu_Q^2)\, \Theta(Q_{n+1}-Q_{\rm cut})\, O_{n+2} \;+\; \dots\;,
\end{aligned}
\tag{3.1}
$$

where again the obvious phase space arguments in the matrix element contributions and splitting kernels have been suppressed for better readability, and where they have been moved to subscripts in the observables. The dots indicate contributions from higher parton-level multiplicities, which are dealt with in an iterative procedure as detailed in section 3.2.

The square bracket on the first line and third line is generated by weighted parton showers, as discussed in section 4.2, while all Sudakov factors $\Delta^{(\mathrm{PS})}$ are generated by standard shower algorithms. The terms $\mathrm{d}\Phi_n \bar{\mathrm{B}}_n^{(\mathrm{A})}$ and $\mathrm{d}\Phi_{n+1}\mathrm{H}_n^{(\mathrm{A})}$ correspond to the fixed-order seed events. A convenient Monte-Carlo algorithm to generate the factor $\mathrm{B}_n/\bar{\mathrm{B}}_n^{(\mathrm{A})}$ will be discussed in section 4.

It is easy to show that next-to-leading order accuracy is maintained for observables sensitive to Φ_{n+1} at $Q > Q_{\rm cut}$, where Q is the transverse momentum scale of the first emission, i.e. of parton $n+1$. Expanding the Sudakov form factor $\Delta_n^{(\mathrm{PS})}(t,\mu_Q^2)$ in the third line to first order and combining it with the square bracket on the same line yields correction terms which are at most of $\mathcal{O}(\alpha_s^2)$.

In order to show the logarithmic accuracy of the procedure, eq. (3.1) is rewritten as follows

$$
\langle O\rangle \;=\; \langle O\rangle^{\rm MC@NLO} \;+\; \langle O\rangle^{\rm corr}\,, \tag{3.2}
$$

JHEP01(2013)144

with $\langle O\rangle^{\text{MC@NLO}}$ given by (2.9). Taking into account only $n+1$ parton final states the correction term this time is given by[3]

$$\begin{aligned}
\langle O\rangle^{\text{corr}} =& \int \mathrm{d}\Phi_{n+1}\,\Theta(Q_{n+1}-Q_{\text{cut}})\,O_{n+1}\,\Delta^{(\text{PS})}_{n+1}(t_c,t_{n+1})\Delta^{(\text{PS})}_{n}(t_{n+1},\mu_Q^2)\\
&\times\left\{\bar{\mathrm{B}}^{(\text{A})}_{n+1}\left(1+\frac{\mathrm{B}_{n+1}}{\bar{\mathrm{B}}^{(\text{A})}_{n+1}}\int_{t_{n+1}}^{\mu_Q^2}\mathrm{d}\Phi_1\,\mathrm{K}_n\right)\frac{\Delta^{(\text{A})}_{n+1}(t_c,t_{n+1})}{\Delta^{(\text{PS})}_{n+1}(t_c,t_{n+1})}-\mathrm{H}^{(\text{A})}_n-\frac{\bar{\mathrm{B}}^{(\text{A})}_n}{\mathrm{B}_n}\,\mathrm{D}^{(\text{A})}_n\,\frac{\Delta^{(\text{A})}_{n}(t_{n+1},\mu_Q^2)}{\Delta^{(\text{PS})}_{n}(t_{n+1},\mu_Q^2)}\right\}\\
&\quad=\int \mathrm{d}\Phi_{n+1}\,\Theta(Q_{n+1}-Q_{\text{cut}})\,O_{n+1}\,\Delta^{(\text{PS})}_{n}(t_{n+1},\mu_Q^2)\\
&\times\left\{\mathrm{D}^{(\text{A})}_n\left[1-\frac{\bar{\mathrm{B}}^{(\text{A})}_n}{\mathrm{B}_n}\,\frac{\Delta^{(\text{A})}_{n}(t_{n+1},\mu_Q^2)}{\Delta^{(\text{PS})}_{n}(t_{n+1},\mu_Q^2)}\right]\right.\\
&\left.\quad-\mathrm{B}_{n+1}\left[1-\left(\frac{\bar{\mathrm{B}}^{(\text{A})}_{n+1}}{\mathrm{B}_{n+1}}+\int_{t_{n+1}}^{\mu_Q^2}\mathrm{d}\Phi_1\,\mathrm{K}_n\right)\frac{\Delta^{(\text{A})}_{n+1}(t_c,t_{n+1})}{\Delta^{(\text{PS})}_{n+1}(t_c,t_{n+1})}\right]\right\}.
\end{aligned}\tag{3.3}$$

Both terms in the curly brackets consist of one factor describing the emission of an extra particle, $\mathrm{D}^{(\text{A})}_n$ and B_{n+1}. Those will eventually yield a contribution of $\mathcal{O}(\alpha_s L^2)$. The factors multiplying these emission terms are at most of $\mathcal{O}(\alpha_s L)$. However, these logarithms, if present, are due to sub-leading colour configurations stemming from the difference between $\Delta^{(\text{A})}$ and $\Delta^{(\text{PS})}$. The combination of virtual and real contributions in $\bar{\mathrm{B}}^{(\text{A})}_n$ does not induce any logarithms spoiling the accuracy of the parton shower. Thus the correction term does not impair the formal logarithmic accuracy of the parton shower.

It is worth noting here that the algorithm detailed in [17], while aiming at the same formal accuracy, follows a different construction paradigm. Rather than starting from the matrix elements, like the approach presented here, and matching the showers to them, its authors start from the parton shower and correct its emissions with higher order matrix elements.

3.2 Iteration for multijet events

Having shown, for the case of the first additional emission, how NLO- and the logarithmic accuracy of the shower are maintained, we now turn to the question how this can also be shown for the kth additional jet. The first thing to be understood is that, in general, the observable O will have support in different sectors by different jet multiplicities. In the formalism outlined here this is reflected by the Θ-functions involving the jet cut Q_{cut} and the scale Q of the softest emission of a given Born-like $(n+k)$-jet configuration, in general given by $Q_{n+k}=Q(\Phi_{n+k})$. For such a configuration, the respective expression for the $(n+k)$-exclusive jet part of the observable,

$$\langle O\rangle^{\text{excl}}_{n+k}=\sum_{j=n+k}^{\infty}\langle O_j\,\Theta(Q_{n+k}-Q_{\text{cut}})\Theta(Q_{\text{cut}}-Q_{n+k+1})\rangle\,,\tag{3.4}$$

[3] Additional contributions are at most of $\mathcal{O}(\alpha_s^2 L^2)$ and thus do not impair the logarithmic or fixed order accuracy we intend to prove.

JHEP01(2013)144

is given by the suitably modified second part of eq. (3.1),

$$\begin{aligned}\langle O\rangle^{\rm excl}_{n+k} &= \int \mathrm{d}\Phi_{n+k}\,\Theta(Q_{n+k}-Q_{\rm cut})\,\bar{\mathrm{B}}^{(\mathrm{A})}_{n+k}\\ &\times\left[\prod_{i=n}^{n+k-1}\Delta^{(\mathrm{PS})}_i(t_{i+1},t_i)\left(1+\frac{\mathrm{B}_{n+k}}{\bar{\mathrm{B}}^{(\mathrm{A})}_{n+k}}\int_{t_{i+1}}^{t_i}\mathrm{d}\Phi_1\,\mathrm{K}_i\right)\right]\\ &\times\left[\Delta^{(\mathrm{A})}_{n+k}(t_c,t_{n+k})\,O_{n+k}+\int_{t_c}^{t_{n+k}}\mathrm{d}\Phi_1\,\frac{\mathrm{D}^{(\mathrm{A})}_{n+k}}{\mathrm{B}_{n+k}}\,\Delta^{(\mathrm{A})}_{n+k}(t_{n+k+1},t_{n+k})\Theta(Q_{\rm cut}-Q_{n+k+1})\,O_{n+k+1}\right]\\ &+\int \mathrm{d}\Phi_{n+k+1}\,\Theta(Q_{n+k}-Q_{\rm cut})\,\Theta(Q_{\rm cut}-Q_{n+k+1})\,O_{n+k+1}\mathrm{H}^{(\mathrm{A})}_{n+k}\prod_{i=n}^{n+k}\Delta^{(\mathrm{PS})}_i(t_{i+1},t_i)\,.\end{aligned}\tag{3.5}$$

In order to see the formal accuracy of this expression, let us define an $(n+k)$-jet inclusive expression of the observable, by dropping the second Θ-function in (3.4). As before, it can be written as the sum of an MC@NLO-like expression acting on the $(n+k)$-parton Born configuration and a correction term,

$$\langle O\rangle^{\rm incl}_{n+k} \;=\; \langle O\rangle^{\rm MC@NLO}_{n+k} \;+\; \langle O\rangle^{\rm corr}_{n+k}\,, \tag{3.6}$$

where

$$\begin{aligned}\langle O\rangle^{\rm MC@NLO}_{n+k} &= \int \mathrm{d}\Phi_{n+k}\,\Theta(Q_{n+k}-Q_{\rm cut})\,\bar{\mathrm{B}}^{(\mathrm{A})}_{n+k}\\ &\times\left[\prod_{i=n}^{n+k-1}\Delta^{(\mathrm{PS})}_i(t_{i+1},t_i)\left(1+\frac{\mathrm{B}_{n+k}}{\bar{\mathrm{B}}^{(\mathrm{A})}_{n+k}}\int_{t_{i+1}}^{t_i}\mathrm{d}\Phi_1\,\mathrm{K}_i\right)\right]\\ &\times\left[\Delta^{(\mathrm{A})}_{n+k}(t_c,t_{n+k})\,O_{n+k}+\int_{t_c}^{t_{n+k}}\mathrm{d}\Phi_1\,\frac{\mathrm{D}^{(\mathrm{A})}_{n+k}}{\mathrm{B}_{n+k}}\,\Delta^{(\mathrm{A})}_{n+k}(t_{n+k+1},t_{n+k})\,O_{n+k+1}\right]\\ &+\int \mathrm{d}\Phi_{n+k+1}\,\Theta(Q_{n+k}-Q_{\rm cut})\,O_{n+k+1}\,\mathrm{H}^{(\mathrm{A})}_{n+k}\prod_{i=n}^{n+k}\Delta^{(\mathrm{PS})}_i(t_{i+1},t_i)\,.\end{aligned}\tag{3.7}$$

The only difference with respect to the usual form of the MC@NLO expression in (2.9) is the term in the second line which encodes a veto on emissions into the jet region from intermediate lines with its $\mathcal{O}(\alpha_s)$-part subtracted.

At the relevant order in α_s, this correction term reads

$$\begin{aligned}\langle O\rangle^{\rm corr}_{n+k} &= \int \mathrm{d}\Phi_{n+k+1}\,\Theta(Q_{n+k+1}-Q_{\rm cut})\,O_{n+k+1}\prod_{i=n}^{n+k+1}\Delta^{(\mathrm{PS})}_i(t_{i+1},t_i)\\ &\times\left\{\mathrm{D}^{(\mathrm{A})}_{n+k}\Theta(t_{n+k}-t_{n+k+1})\left[1-\left(\frac{\bar{\mathrm{B}}^{(\mathrm{A})}_{n+k}}{\mathrm{B}_{n+k}}+\sum_{i=n}^{n+k-1}\int_{t_{i+1}}^{t_i}\mathrm{d}\Phi_1\mathrm{K}_i\right)\frac{\Delta^{(\mathrm{A})}_{n+k}(t_{n+k+1},t_{n+k})}{\Delta^{(\mathrm{PS})}_{n+k}(t_{n+k+1},t_{n+k})}\right]\right.\\ &\left.-\,\mathrm{B}_{n+k+1}\left[1-\left(\frac{\bar{\mathrm{B}}^{(\mathrm{A})}_{n+k+1}}{\mathrm{B}_{n+k+1}}+\sum_{i=n}^{n+k}\int_{t_{i+1}}^{t_i}\mathrm{d}\Phi_1\mathrm{K}_i\right)\frac{\Delta^{(\mathrm{A})}_{n+k+1}(t_c,t_{n+k+1})}{\Delta^{(\mathrm{PS})}_{n+k+1}(t_c,t_{n+k+1})}\right]\right\},\end{aligned}\tag{3.8}$$

JHEP01(2013)144

and the same reasoning already applied to eq. (3.3) yields the desired result. For a more detailed discussion, including the effect of truncated showering, see [19].

The finding above shows that no terms appear due to the merging prescription that violate the logarithmic accuracy of the parton shower at and around Q_{cut}. To see this, it is sufficient to analyse the first emission off the $(n+k)$-jet configuration over the full phase space. The second emission is, of course, completely determined by the parton shower and thus correct by definition. Also, clearly, the phase space for this first emission is confined to the region below Q_{cut}, therefore the behaviour above this scale is defined by the parton-level result with next higher multiplicity, the $(n+k+1)$-jet configuration. By however extending the first emission above this cut and analysing the impact on $\mathcal{O}_{n+k+1}$ we show that the two regions match as smoothly as the logarithmic accuracy of the parton shower dictates.

3.3 Renormalisation scale uncertainties

The key aim of the MePs@Nlo approach presented here is to reduce the dependence of the merged prediction on the renormalisation scale μ_R, which is employed in the computation of the hard matrix elements. This scale has not been made explicit so far.

Note that only the dependence on the renormalisation scale is reduced compared to the MePs method, while the dependence on the resummation scale, μ_Q, remains the same. This is a direct consequence of the fact that the parton-shower evolution is not improved in our prescription, but only the accuracy of the hard matrix elements. The resummation scale dependence was analysed in great detail in [12].

Following the MePs strategy, the renormalisation scale should be determined by analogy of the leading-order matrix element with the respective parton shower branching history [5]. In next-to-leading order calculations, however, one needs a definition which is independent of the parton multiplicity. The same scale should be used in Born matrix elements and real-emission matrix elements if they have similar kinematics, and in particular when the additional parton of the real-emission correction becomes soft or collinear. This can be achieved if we define the renormalisation scale for a process of $\mathcal{O}(\alpha_s^n)$ as [24]

$$\alpha_s(\mu_R^2)^n \;=\; \prod_{i=1}^{n} \alpha_s(\mu_i^2)\;, \tag{3.9}$$

a procedure that has been used in LO merging for some time. Here, μ_i^2 are the respective scales defined by analogy of the Born configuration with a parton-shower branching history.[4]

The renormalisation scale uncertainty in the MePs@Nlo approach is then determined by varying $\mu_R \to \tilde{\mu}_R$, while simultaneously correcting for the one-loop effects induced by a redefinition in eq. (3.9). That is, the Born matrix element is multiplied by

$$\alpha_s(\tilde{\mu}_R^2)^n \left(1 - \frac{\alpha_s(\tilde{\mu}_R^2)}{2\pi}\,\beta_0 \sum_{i=1}^{n} \log\frac{\mu_i^2}{\tilde{\mu}_R^2}\right), \tag{3.10}$$

to generate the one-loop counter-term, while higher-order contributions remain the same.

[4] In the case of the real-emission correction and the corresponding dipole subtraction terms we consider the underlying Born configuration instead. The same scale definition is used in the parton shower and, consequently, in the Sudakov form factors. Of course, the nodal scales μ_i found in the backward clustering on the Born-like configuration of a single event then enter the truncated showering.

JHEP01(2013)144

4 Monte-Carlo implementation

In this section we describe the Monte Carlo implementation of the merging formula eq. (3.1) in SHERPA. The techniques needed to combine leading-order matrix elements with parton showers are given elsewhere [5].

4.1 Generation of the parton-shower counterterm

In addition, we now have to implement a method to generate the parton-shower counterterm on the third line of eq. (3.1). Note that, by construction, this counterterm has the same functional form as the exponent of the Sudakov form factor $\Delta_n^{(\mathrm{PS})}(t,\mu_Q^2)$. We can therefore use the following algorithm:

- start from an n-parton configuration underlying the $n+1$-parton event at scale μ_Q^2, and implement a truncated parton shower with lower cutoff scale t.
- If no emission is produced, the original $n+1$-parton configuration is retained.
- If the first emission is generated at scale t' with $Q > Q_{\mathrm{cut}}$, the event weight is multiplied by $1/\kappa$, where $\kappa = \bar{\mathrm{B}}_{n+1}^{(\mathrm{A})}(\Phi_{n+1})/\mathrm{B}_{n+1}(\Phi_{n+1})$. Evolution is restarted at t'.
- All subsequent emissions are treated as in a standard truncated vetoed parton shower.

Events will then be distributed as

$$\begin{aligned}\Delta_n^{(\mathrm{PS})}(t,\mu_Q^2) + \frac{1}{\kappa}\int_t^{\mu_Q^2} \mathrm{d}\Phi_1 \left[\mathrm{K}_n(\Phi_1)\,\Theta(Q-Q_{\mathrm{cut}})\,\Delta_n^{(\mathrm{PS})}(t',\mu_Q^2)\right]\Delta_n^{(\mathrm{PS})}(t,t') \\ = \Delta_n^{(\mathrm{PS})}(t,\mu_Q^2)\left[1+\frac{1}{\kappa}\int_t^{\mu_Q^2}\mathrm{d}\Phi_1\,\mathrm{K}_n(\Phi_1)\,\Theta(Q-Q_{\mathrm{cut}})\right].\end{aligned} \tag{4.1}$$

This simple algorithm allows to identify the $\mathcal{O}(\alpha_s)$ counterterm with an omitted emission and to generate the correction term on-the-flight, much like the Sudakov form factor is computed in any parton-shower algorithm itself.

4.2 Generation of the MC@NLO Sudakov form factor

In this subsection we briefly recall an algorithm to compute MC@NLO Sudakov form factors [12], which is one of the basic ingredients to our method.

It is well known how to generate emissions according to Sudakov form factors with strictly negative exponent. In our implementation of MC@NLO, however, we have to deal with potentially positive exponents, related to subleading colour configurations. This leads to form factors larger than one, which cannot be interpreted in terms of no-branching probabilities and which are dealt with using a modified Sudakov veto algorithm [12, 25].

Assume that $f(t)$ is the sole splitting kernel in our parton shower, integrated over z and ϕ. The differential probability for generating a branching at scale t, when starting from an upper evolution scale t' is then given by

$$\mathcal{P}(t,t') \;=\; f(t)\,\exp\left\{-\int_t^{t'}\mathrm{d}\bar{t}\,f(\bar{t})\right\}. \tag{4.2}$$

The key point of the veto algorithm is, that even if the primitive of $f(t)$ is unknown, one can still generate events according to $\mathcal{P}$ using an overestimate $g(t) \geq f(t)$, if $g(t)$ has a known integral. Firstly, a value t is generated as $t = G^{-1}\left[G(t') + \log \# \right]$. Secondly, the value is accepted with probability $f(t)/g(t)$ [26].

One can now introduce an additional estimate $h(t)$, which is not necessarily an overestimate of $f(t)$. The related weights are applied analytically rather than using a hit-or-miss method. They can thus be used to absorb the negative sign of the MC@NLO kernels $\mathrm{D}_n^{(\mathrm{A})}/\mathrm{B}_n$. This leads to a correction factor for one accepted branching with m intermediate rejections of

$$w(t, t_1, \ldots, t_m) \;=\; \frac{g(t)}{h(t)} \prod_{i=1}^{m} \frac{g(t_i)}{h(t_i)} \frac{h(t_i) - f(t_i)}{g(t_i) - f(t_i)} \;, \tag{4.3}$$

where the t_i run over intermediately rejected steps. Note that eq. (4.3) can lead to negative weights, which reflect the fact that sub-leading colour configurations are taken into account and that the a-priori density $h(t)$ might underestimate $f(t)$.

In order to implement an evolution using the MC@NLO kernels $\mathrm{D}_n^{(\mathrm{A})}/\mathrm{B}_n$ we need to identify the function f above with the (z, ϕ)-integral of these kernels. A convenient choice of the function h will be the (z, ϕ)-integral of the parton-shower evolution kernels K_n. We are then free to choose the auxiliary function g on a point-by-point basis, but a convenient way is to define $g = C\, f$, where C is a constant larger than one. This guarantees that both acceptance and rejection terms are generated in sufficient abundance to reduce statistical fluctuations.

The above method guarantees that all subleading colour single logarithmic corrections to B_n are exponentiated. One can therefore guarantee a process-independent exponentiation of next-to-leading colour real-emission corrections in the MC@NLO.

5 Results

In this section results obtained with the MEPS@NLO method are presented for the case of e^+e^--annihilation into hadrons. The general-purpose event generator SHERPA sets the framework for this study [15, 16]. Leading-order matrix elements are generated with AMEGIC++ [27] and COMIX [28]. Automated dipole subtraction [29] and the Binoth–Les Houches interface [30] are employed to obtain parton-level events at next-to-leading order with virtual corrections provided by the BLACKHAT library [31–34]. The parton shower in SHERPA is based on Catani-Seymour dipole factorisation [35]; the related MC@NLO generator has been presented in [12]. In contrast to all other MC@NLO implementations, no leading colour approximation is made in the first step of the parton shower, cf. section 4.2. The resummation scale is determined on an event-by-event basis by backward clustering as described in [5]. In the special case of e^+e^- collisions discussed here this simplifies to the centre-of-mass energy. The results presented here are at the hadron level. Note that the hadronisation model in SHERPA [36] has been tuned in conjunction with the parton shower and leading order matrix elements. It is therefore not surprising when deviations are found in observables that are sensitive to soft particle dynamics. In the future this

JHEP01(2013)144

will necessitate a new tune of the hadronisation based on the NLO-merging outlined here, rather than on the LO MEPS prescription that has been used so far in Sherpa.

For each of the inclusive samples discussed in the following we generated $40 \cdot 10^6$ weighted events. The sub-contributions in different jet multiplicities were automatically chosen according to their cross sections. Within each jet multiplicity, the number of $\mathbb{H}$-events was statistically enhanced by a factor of 10 with respect to the $\mathbb{S}$-events. The cross section fraction of negative events was 1.3% for Mc@Nlo, 0.4% for MEnloPS, and 10.4% for MePs@Nlo. The generation of $40 \cdot 10^6$ events needed 1.6 CPU days (Mc@Nlo), 1.7 CPU days (MEnloPS) and 2.0 CPU days (MePs@Nlo) on Intel Xeon E5440 CPUs at 2.83GHz.

5.1 Choice of the merging scale

Figure 1 shows the dependence of MePs@Nlo predictions for the Durham jet resolution on the merging scale Q_{cut}. In order to match the customary notation we quote $Y_{\text{cut}} = (Q_{\text{cut}}/E_{\text{cms}})^2$. All results were generated using 2-,3- and 4-jet NLO parton-level calculations combined with 5- and 6-jet at leading order. The variation of results with Y_{cut} in the region below and around Y_{cut} is of the order of 10%, the predictions above the cut are remarkably stable and match the experimental data very well. Consequently, one should always choose the merging cut such that the analysis region is fully contained in the region covered by the NLO calculation of interest.

5.2 Comparison of approaches and their perturbative uncertainties

In this section we compare the renormalisation scale uncertainties between the MEnloPS and the MePs@Nlo method. We choose $\tilde{\mu}_R = C\mu_R$ with $C \in \{0.5, 1, 2\}$ and set $Y_{\text{cut}} = 2$. In the MePs@Nlo sample we generate 2-,3-, and 4-parton final states at NLO and 5- and 6-parton final states at LO. The MEnloPS sample only has the 2-parton final state at NLO and the remaining multiplicities up to 6 partons from tree-level matrix elements. Figures 2 to 8 show the respective scale variations as bands around the central prediction with $C = 1$. A significant reduction of the scale uncertainty is found for those observables, which are sensitive to the NLO parton-level results. This can be seen in particular in figure 2, where the $2 \to 3$ and $3 \to 4$-jet rates show significantly reduced uncertainties for larger y, while the $4 \to 5$ and $5 \to 6$-jet rates do not. Similar effects are observed in most event shape distributions in the hard region, for example in figure 3, for $T \to 0.5$. The reduction of the scale uncertainty in the moments of the event shape distributions in particular is more than impressive. It is also worth pointing out that the typical Sudakov shoulder at $C = 0.75$ in the C-parameter, which is notoriously difficult to describe in fixed-order calculations, now shows a remarkably smooth behaviour due to the successful interplay of the different multiplicity contributions.

A final comment, concerning the evaluation of theory uncertainties by scale variations is in order here. Clearly, there are two sources of perturbative uncertainties: the one analysed here, which stems from the matrix element. It is thus susceptible to variations of the renormalisation and, if present, the factorisation scale. In addition, changes in the value of

JHEP01(2013)144

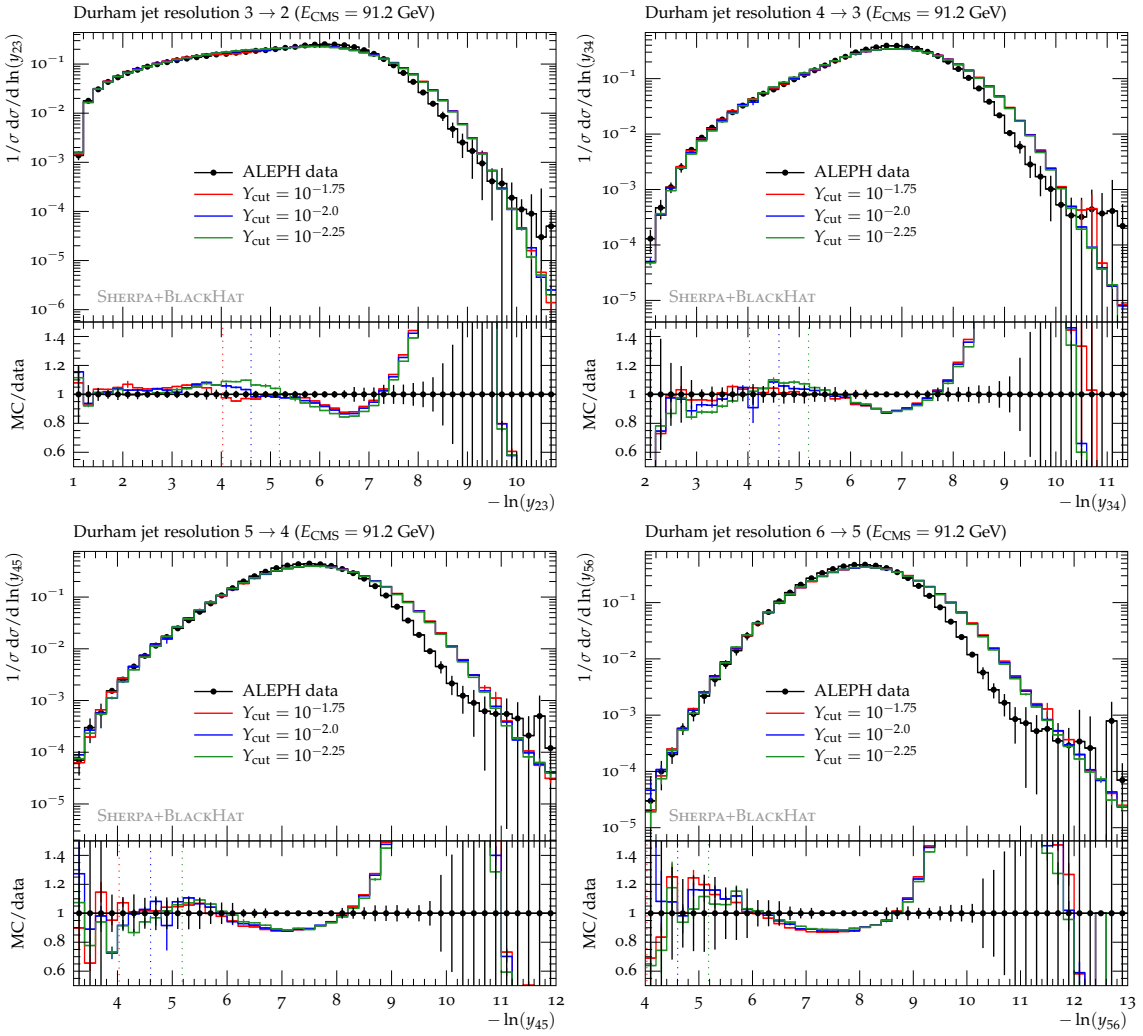

Figure 1. Experimental data from ALEPH [37] for the differential $(n+1) \to n$ jet rates with $n = \{2, 3, 4, 5\}$ (upper and lower panel, left to right) at the Z pole ($E_{\text{c.m.}} = 91.2\,\text{GeV}$) are compared with MePs@Nlo simulations with different values of the merging cut, $Y_{\text{cut}} = 10^{-\{1.75,\,2.0,\,2.25\}}$. To guide the eye, the merging cuts have been indicated with dotted lines in the same colour in the ratio plot.

α_s, which we did not pursue here, or in parton distribution functions would have to be considered for a more complete assessment of such uncertainties. On the other hand, there are, of course, also uncertainties in the treatment of secondary emissions through the parton shower. There, in addition to the variations outlined above, one could also vary the parton shower starting scale, μ_Q, which is equivalent to a variation of the corresponding resummation scale in analytical calculations. Obviously in regions that are dominated by the parton shower, such a variation would give a more sensible estimate of theory uncertainties than a variation of the scales in the matrix element, that we focused on here. As an example for this, consider the low-$p_\perp$ regime of the differential jet rates y_{ij}, $-\log y_{ij} \to \infty$. There the

JHEP01(2013)144

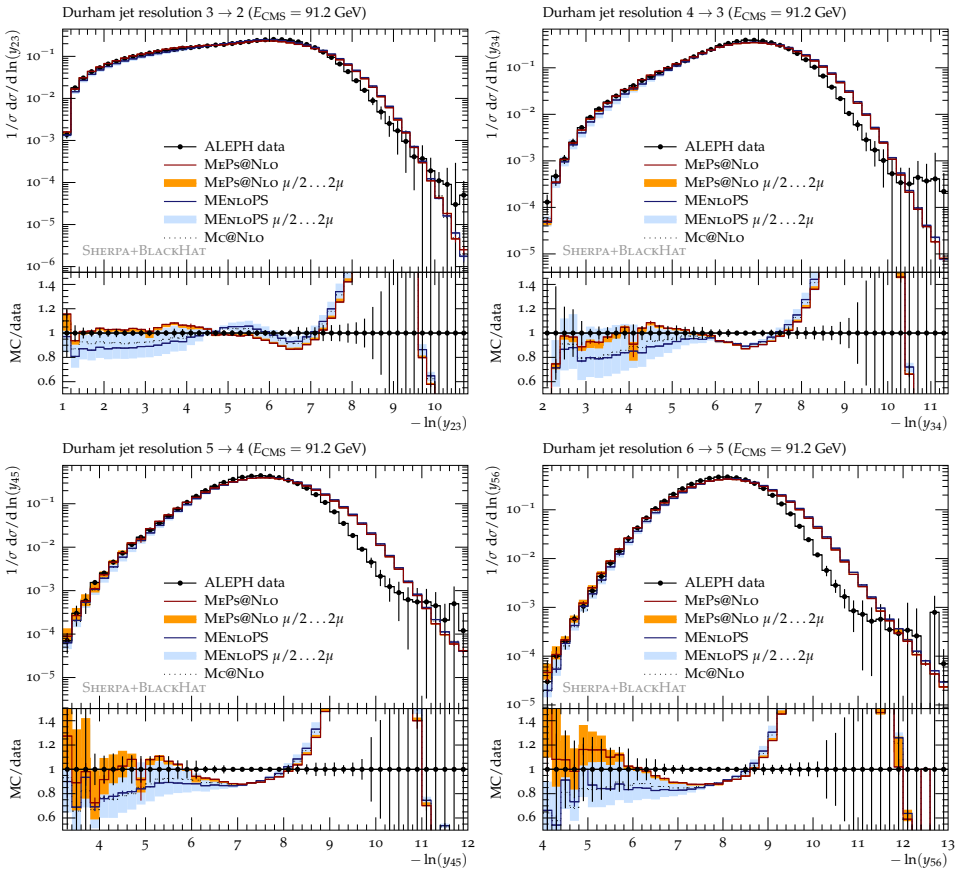

Figure 2. Perturbative uncertainties in MENLOPS and MEPS@NLO predictions of differential jet rates compared to data from ALEPH [37].

bands obtained from a scale variation in the matrix element regime are suspiciously small, and it is clear that a variation of the resummation scale would yield larger uncertainties. Another important source of uncertainty is the model for parton to hadron fragmentation. The same, obviously is true for the MEPS@NLO and the MENLOPS method, since in the small-y region both exhibit a comparable formal accuracy. A careful analysis of such effects, however, is beyond the focus of this paper, which discusses improvements of our ability to generate inclusive samples of events by increasing the formal accuracy of the matrix element part of the simulation. We therefore postpone this discussion to future work.

6 Conclusions

In this paper we have introduced a method for a consistent multijet merging at NLO accuracy for the case of e^+e^--annihilations to hadrons. By explicit calculation, we have shown that our description maintains the higher order accuracy of the underlying matrix elements in their respective phase space range, while the logarithmic accuracy of the parton shower is respected. We have also analysed the impact of renormalisation scale variations in our

JHEP01(2013)144

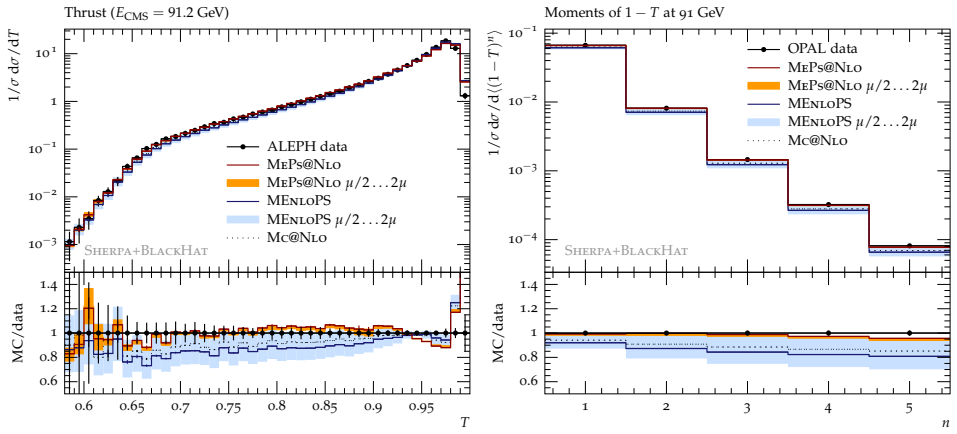

Figure 3. Perturbative uncertainties in MENLOPS and MEPS@NLO predictions of thrust. Compared are the measurements for the event shape from ALEPH [37] and its moments from OPAL [38].

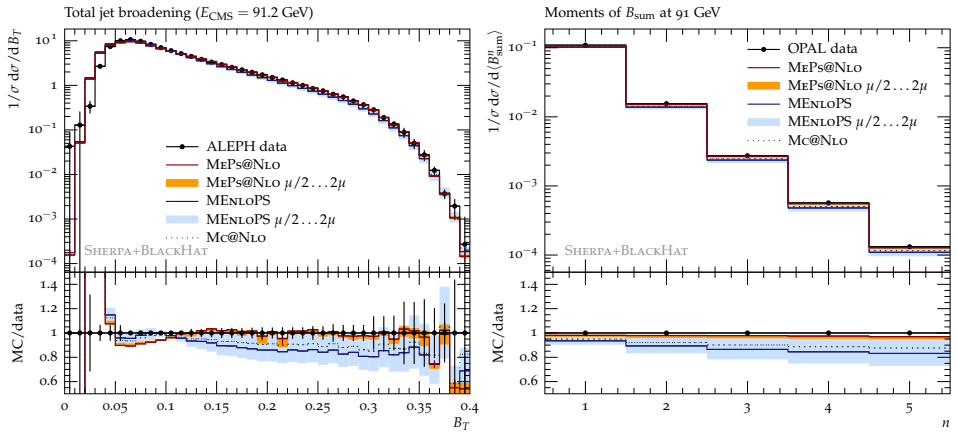

Figure 4. Perturbative uncertainties in MENLOPS and MEPS@NLO predictions of total jet/hemisphere broadening. Compared are the measurements from ALEPH [37] and OPAL [38].

new formalism. The results displayed here are exemplary for a far wider range of observables, which show a very good agreement between our simulation and data throughout. The most remarkable feature of our formalism is the greatly reduced uncertainty due to variations of the renormalisation scale. We have also implemented our formalism for the case of collisions with hadronic initial states [19], where we find a similar behaviour.

Acknowledgments

SH's work was supported by the US Department of Energy under contract DE-AC02-76SF00515, and in part by the US National Science Foundation, grant NSF-PHY-0705682, (The LHC Theory Initiative). MS's work was supported by the Research Executive Agency (REA) of the European Union under the Grant Agreement number PITN-GA-2010-264564

JHEP01(2013)144

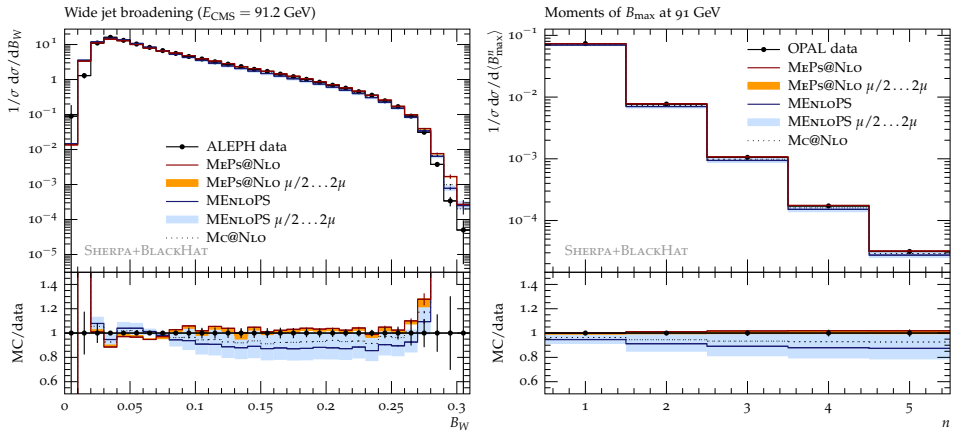

Figure 5. Perturbative uncertainties in MENLOPS and MEPS@NLO predictions of wide jet/hemisphere broadening. Compared are the measurements from ALEPH [37] and OPAL [38].

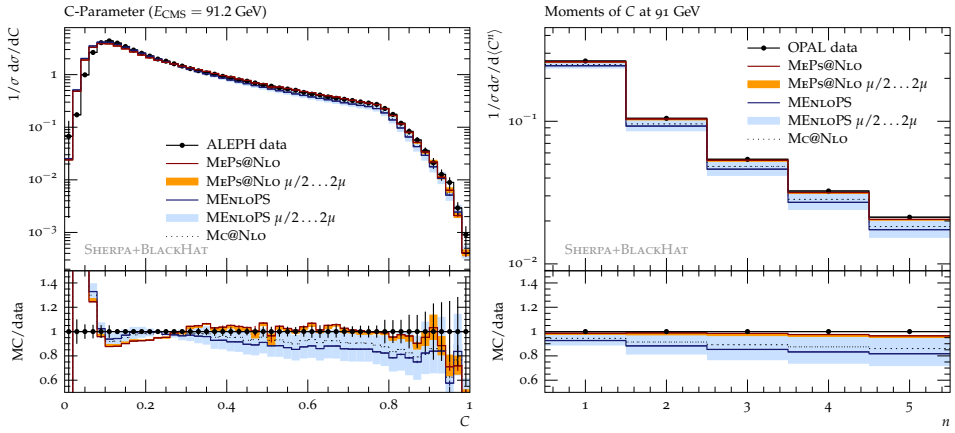

Figure 6. Perturbative uncertainties in MENLOPS and MEPS@NLO predictions of the C-parameter. Compared are the measurements from ALEPH [37] and OPAL [38].

(LHCPhenoNet). FS's work was supported by the German Research Foundation (DFG) via grant DI 784/2-1. This research is also supported in part by the Swiss National Science Foundation (SNF) under contracts 200020-138206, and by the Research Executive Agency (REA) of the European Union under the Grant Agreement number PITN-GA-2010-264564 (LHCPhenoNet).

TG and SH would like to acknowledge the Kavli Institute for Theoretical Physics (KITP) at UC Santa Barbara for its hospitality during the 2011 program "Harmony of Scattering Amplitudes".

We gratefully thank the bwGRiD project for computational resources.

JHEP01(2013)144

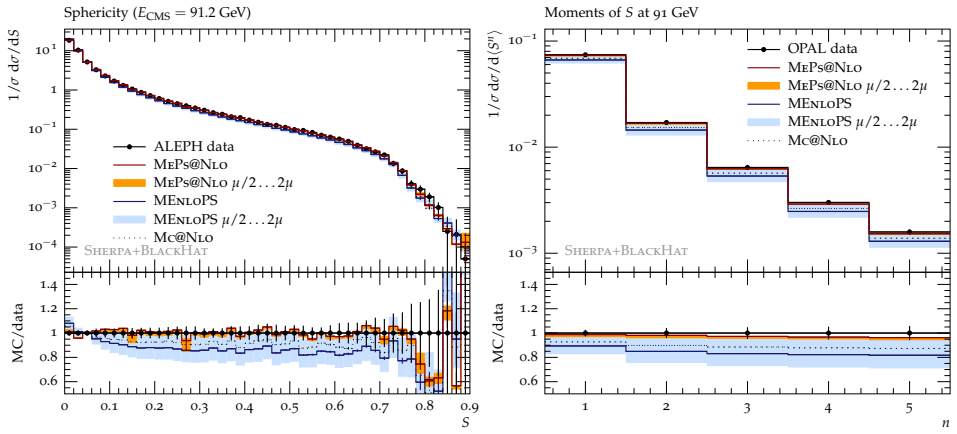

Figure 7. Perturbative uncertainties in MENLOPS and MEPS@NLO predictions of sphericity. Compared are the measurements from ALEPH [37] and OPAL [38].

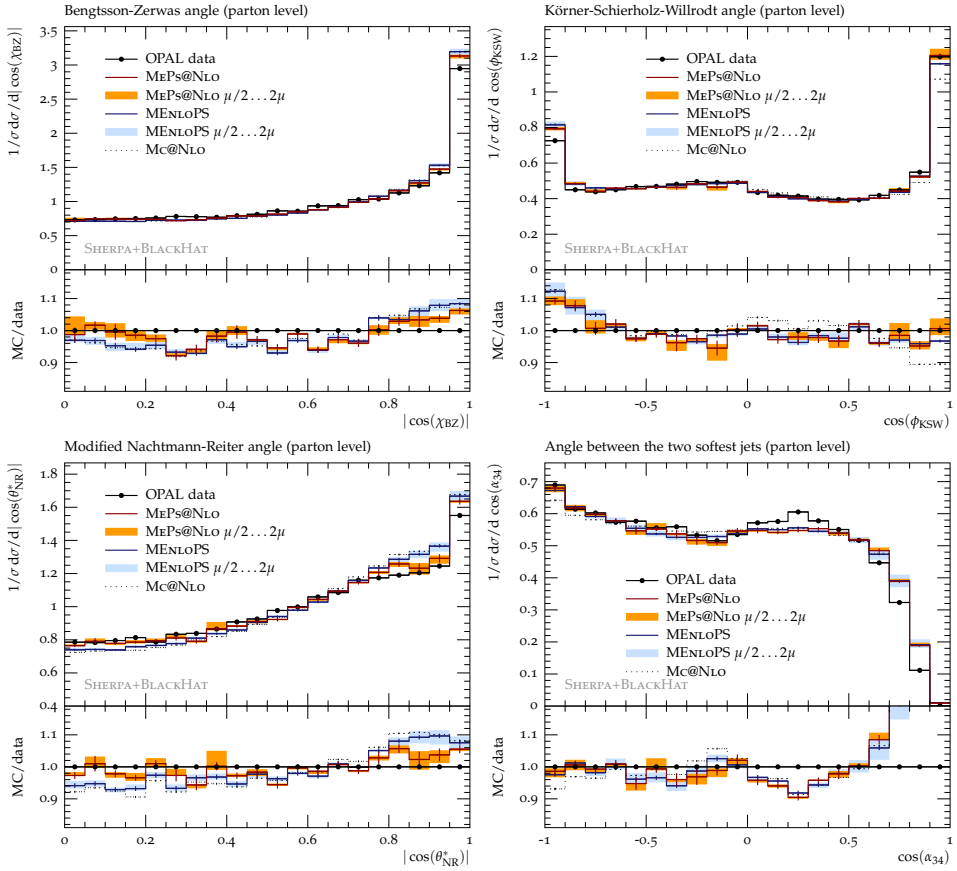

Figure 8. Four-jet angles using the Durham algorithm compared to data from OPAL [39].

References

[1] S. Catani, F. Krauss, R. Kuhn and B. Webber, *QCD matrix elements + parton showers*, *JHEP* **11** (2001) 063 [hep-ph/0109231] [INSPIRE].

JHEP01(2013)144

[2] L. Lönnblad, *Correcting the color dipole cascade model with fixed order matrix elements*, *JHEP* **05** (2002) 046 [hep-ph/0112284] [INSPIRE].

[3] M.L. Mangano, M. Moretti and R. Pittau, *Multijet matrix elements and shower evolution in hadronic collisions: $Wb\bar{b}$ + n jets as a case study*, *Nucl. Phys.* **B 632** (2002) 343 [hep-ph/0108069] [INSPIRE].

[4] F. Krauss, *Matrix elements and parton showers in hadronic interactions*, *JHEP* **08** (2002) 015 [hep-ph/0205283] [INSPIRE].

[5] S. Hoeche, F. Krauss, S. Schumann and F. Siegert, *QCD matrix elements and truncated showers*, *JHEP* **05** (2009) 053 [arXiv:0903.1219] [INSPIRE].

[6] K. Hamilton, P. Richardson and J. Tully, *A modified CKKW matrix element merging approach to angular-ordered parton showers*, *JHEP* **11** (2009) 038 [arXiv:0905.3072] [INSPIRE].

[7] W. Giele, D. Kosower and P. Skands, *Higher-order corrections to timelike jets*, *Phys. Rev.* **D 84** (2011) 054003 [arXiv:1102.2126] [INSPIRE].

[8] L. Lönnblad and S. Prestel, *Matching tree-level matrix elements with interleaved showers*, *JHEP* **03** (2012) 019 [arXiv:1109.4829] [INSPIRE].

[9] S. Frixione and B.R. Webber, *Matching NLO QCD computations and parton shower simulations*, *JHEP* **06** (2002) 029 [hep-ph/0204244] [INSPIRE].

[10] P. Nason, *A new method for combining NLO QCD with shower Monte Carlo algorithms*, *JHEP* **11** (2004) 040 [hep-ph/0409146] [INSPIRE].

[11] R. Frederix et al., *aMC@NLO predictions for Wjj production at the Tevatron*, *JHEP* **02** (2012) 048 [arXiv:1110.5502] [INSPIRE].

[12] S. Hoeche, F. Krauss, M. Schonherr and F. Siegert, *A critical appraisal of NLO+PS matching methods*, *JHEP* **09** (2012) 049 [arXiv:1111.1220] [INSPIRE].

[13] K. Hamilton and P. Nason, *Improving NLO-parton shower matched simulations with higher order matrix elements*, *JHEP* **06** (2010) 039 [arXiv:1004.1764] [INSPIRE].

[14] S. Hoche, F. Krauss, M. Schonherr and F. Siegert, *NLO matrix elements and truncated showers*, *JHEP* **08** (2011) 123 [arXiv:1009.1127] [INSPIRE].

[15] T. Gleisberg et al., *SHERPA 1.α: a proof of concept version*, *JHEP* **02** (2004) 056 [hep-ph/0311263] [INSPIRE].

[16] T. Gleisberg et al., *Event generation with SHERPA 1.1*, *JHEP* **02** (2009) 007 [arXiv:0811.4622] [INSPIRE].

[17] N. Lavesson and L. Lönnblad, *Extending CKKW-merging to one-loop matrix elements*, *JHEP* **12** (2008) 070 [arXiv:0811.2912] [INSPIRE].

[18] S. Alioli, K. Hamilton and E. Re, *Practical improvements and merging of POWHEG simulations for vector boson production*, *JHEP* **09** (2011) 104 [arXiv:1108.0909] [INSPIRE].

[19] S. Hoeche, F. Krauss, M. Schonherr and F. Siegert, *QCD matrix elements + parton showers: the NLO case*, arXiv:1207.5030 [INSPIRE].

[20] S. Hoche, F. Krauss, M. Schonherr and F. Siegert, *Automating the POWHEG method in SHERPA*, *JHEP* **04** (2011) 024 [arXiv:1008.5399] [INSPIRE].

JHEP01(2013)144

[21] S. Catani and M. Seymour, *A general algorithm for calculating jet cross-sections in NLO QCD*, *Nucl. Phys.* **B 485** (1997) 291 [*Erratum ibid.* **B 510** (1998) 503] [hep-ph/9605323] [INSPIRE].

[22] S. Catani, S. Dittmaier and Z. Trócsányi, *One loop singular behavior of QCD and SUSY QCD amplitudes with massive partons*, *Phys. Lett.* **B 500** (2001) 149 [hep-ph/0011222] [INSPIRE].

[23] S. Frixione, P. Nason and C. Oleari, *Matching NLO QCD computations with parton shower simulations: the POWHEG method*, *JHEP* **11** (2007) 070 [arXiv:0709.2092] [INSPIRE].

[24] K. Hamilton, P. Nason and G. Zanderighi, *MINLO: multi-Scale Improved NLO*, *JHEP* **10** (2012) 155 [arXiv:1206.3572] [INSPIRE].

[25] S. Hoeche, S. Schumann and F. Siegert, *Hard photon production and matrix-element parton-shower merging*, *Phys. Rev.* **D 81** (2010) 034026 [arXiv:0912.3501] [INSPIRE].

[26] T. Sjöstrand, S. Mrenna and P.Z. Skands, *PYTHIA* 6.4 *physics and manual*, *JHEP* **05** (2006) 026 [hep-ph/0603175] [INSPIRE].

[27] F. Krauss, R. Kuhn and G. Soff, *AMEGIC++* 1.0*: a matrix element generator in C++*, *JHEP* **02** (2002) 044 [hep-ph/0109036] [INSPIRE].

[28] T. Gleisberg and S. Hoeche, *Comix, a new matrix element generator*, *JHEP* **12** (2008) 039 [arXiv:0808.3674] [INSPIRE].

[29] T. Gleisberg and F. Krauss, *Automating dipole subtraction for QCD NLO calculations*, *Eur. Phys. J.* **C 53** (2008) 501 [arXiv:0709.2881] [INSPIRE].

[30] T. Binoth et al., *A proposal for a standard interface between Monte Carlo tools and one-loop programs*, *Comput. Phys. Commun.* **181** (2010) 1612 [arXiv:1001.1307] [INSPIRE].

[31] C. Berger et al., *An automated implementation of on-shell methods for one-loop amplitudes*, *Phys. Rev.* **D 78** (2008) 036003 [arXiv:0803.4180] [INSPIRE].

[32] C. Berger et al., *Next-to-leading order QCD predictions for W+3-jet distributions at hadron colliders*, *Phys. Rev.* **D 80** (2009) 074036 [arXiv:0907.1984] [INSPIRE].

[33] C. Berger et al., *Next-to-leading order QCD predictions for $Z, \gamma^* + 3$-jet distributions at the Tevatron*, *Phys. Rev.* **D 82** (2010) 074002 [arXiv:1004.1659] [INSPIRE].

[34] C. Berger et al., *Precise predictions for W+4 jet production at the Large Hadron Collider*, *Phys. Rev. Lett.* **106** (2011) 092001 [arXiv:1009.2338] [INSPIRE].

[35] S. Schumann and F. Krauss, *A parton shower algorithm based on Catani-Seymour dipole factorisation*, *JHEP* **03** (2008) 038 [arXiv:0709.1027] [INSPIRE].

[36] J.-C. Winter, F. Krauss and G. Soff, *A modified cluster hadronization model*, *Eur. Phys. J.* **C 36** (2004) 381 [hep-ph/0311085] [INSPIRE].

[37] ALEPH collaboration, A. Heister et al., *Studies of QCD at e^+e^- centre-of-mass energies between* 91 *GeV and* 209 *GeV*, *Eur. Phys. J.* **C 35** (2004) 457 [INSPIRE].

[38] OPAL collaboration, G. Abbiendi et al., *Measurement of event shape distributions and moments in $e^+e^- \to$ hadrons at* 91–209 *GeV and a determination of α_s*, *Eur. Phys. J.* **C 40** (2005) 287 [hep-ex/0503051] [INSPIRE].

[39] OPAL collaboration, G. Abbiendi et al., *A simultaneous measurement of the QCD color factors and the strong coupling*, *Eur. Phys. J.* **C 20** (2001) 601 [hep-ex/0101044] [INSPIRE].

JHEP01(2013)144